

Tribology Aspects in Angular Transmission Systems

Part I

GENERAL EXPLANATIONS ON THEORETICAL BEVEL GEAR ANALYSIS

Dr. Hermann Stadtfeld

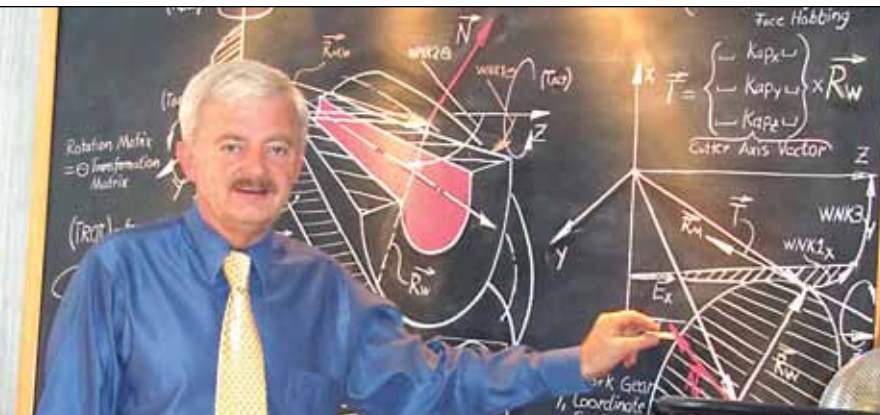
(This article is the first of an eight-part series. Each article will be presented first and exclusively by Gear Technology, and the entire series will be included in Dr. Stadtfeld's upcoming book on the subject, which is scheduled for release in both English and German versions by The Gleason Works in 2011.)

Introduction

Bevel and hypoid gears are complex, three-dimensional gearing systems with flank forms not easily described in conjunction with a mathematical function. As early as the 1970s, computer programs have existed to define

the flank surfaces of bevel and hypoid gears. The latest bevel and hypoid gear analysis programs employ a simulation of the manufacturing process based on a virtual bevel gear generator—i.e., a virtual basic machine. This basic machine provides the correct definition of the workpiece blank, the cutting tool and all the freedoms between work and tool of a universal bevel gear generator (Fig. 1). As such, the input data define not only the work and tool but also the geometric and kinematic relationship during a pinion or a gear manufacturing process. The cutting tool represents one tooth of a generating gear while it rotates around the cutter head axis. The rotation of the cutter head center around the generating cradle axis represents the rotation of the generating gear, which is in mesh with the work gear. This in turn requires that the work gear rotates with the correct ratio between generating gear and work gear. The results of the manufacturing simulation are the surfaces of pinion and gear teeth, described as the points and normal vectors of the surface grids. These surfaces are the basis of a number of analyses, such as tooth contact analysis (TCA), sliding and rolling velocity calculation and more.

The analysis results—like ease-off and tooth contact—are plotted within the projected



Dr. Hermann Stadtfeld received a bachelor's degree in 1978 and in 1982 a master's degree in mechanical engineering at the Technical University in Aachen, Germany. He then worked as a scientist at the Machine Tool Laboratory of the Technical University of Aachen. In 1987, he received his Ph.D. and accepted the position as head of engineering and R&D of the Bevel Gear Machine Tool Division of Oerlikon Buehrle AG in Zurich, Switzerland. In 1992, Dr. Stadtfeld accepted a position as visiting professor at the Rochester Institute of Technology. From 1994 until 2002, he worked for The Gleason Works in Rochester, New York—first as director of R&D and then as vice president of R&D. After an absence from Gleason between 2002 to 2005, when Dr. Stadtfeld established a gear research company in Germany and taught gear technology as a professor at the University of Ilmenau, he returned to the Gleason Corporation, where he holds today the position of vice president-bevel gear technology and R&D. Dr. Stadtfeld has published more than 200 technical papers and eight books on bevel gear technology. He holds more than 40 international patents on gear design and gear process, as well as tools and machines.

ring gear tooth boundaries. Figure 2 provides the graphical explanation of the projection plane. The tooth corner points are transferred into an axial plane. Each point on a flank surface corresponds to a point on the projection plane. The projection plane is utilized in two- and three-dimensional graphics (as indicated, right) in order to ensure certain qualitative and quantitative properties are graphically visible. Those properties result from the interaction between a pinion flank and its mating gear flank. The analysis results—by definition—are only shown in the gear projection plane. The orientation within the tooth is defined as “length direction,” corresponding to XG, and “profile direction,” corresponding to YG (Fig. 2). Also, the definitions of “toe” and “heel,” as well as “top” and “root,” are provided.

A theoretical tooth contact analysis prior to gear manufacturing can be performed in order to observe the effect of the crowning in connection with the basic characteristics of a particular gear set.

Tooth Contact Analysis

Figure 3 shows the result of a tooth contact analysis of a conjugate spiral bevel gear set. The two columns in Figure 3 represent the analysis results of the coast side (left, vertical sequence) and the drive side (right, vertical sequence). The drive side is the flank pair, where the pinion concave flank meshes with the gear convex flank. The reverse direction is called the coast side. In the drive side direction, the pinion deflects away from the ring gear—which is, among other factors, the preferred condition. Transmission of torque and speed on the coast side leads to a pinion deflection toward the ring gear, thus reducing backlash in extreme cases to zero. Since this situation occurs under high load and interrupts any lubrication, it leads to surface damages that can result in tooth fracture. The recommended backlash in bevel gear sets is 0.03 times the module.

The example in Figure 3 is the analysis results of a conjugate bevel gear set—the basis of all gearing. Each flank surface point of the pinion interacts with a corresponding gear flank surface point, in accordance with gearing law—i.e., it transmits the ratio given by the quotient of the pinion and gear tooth count perfectly.

The top graphics in Figure 3 show the so-called ease-off topography in a three-dimensional representation (above the projection of

the gear tooth area). The ease-off shows the consolidated amounts of crowning applied to the pinion and gear flank surfaces (versus the theoretically precise flanks). In this example of a conjugate gearset, the ease-off values above the presentation plane are zero.

continued

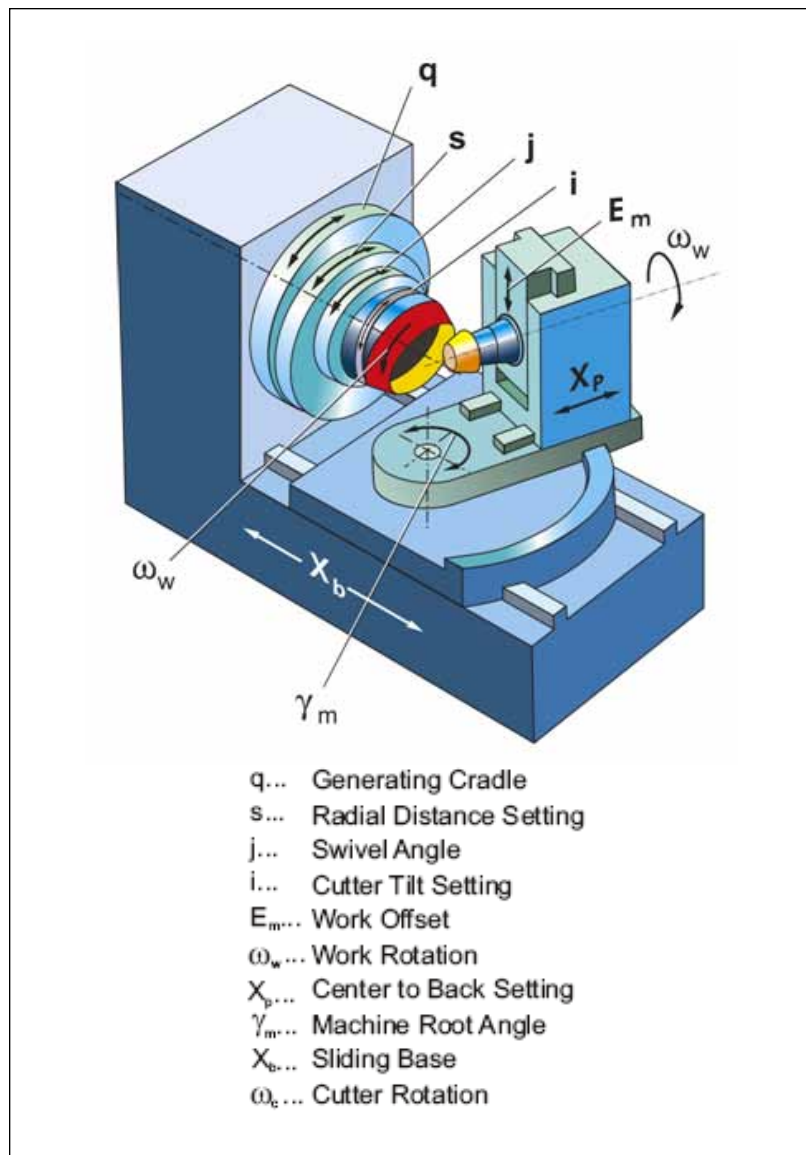


Figure 1—Universal model for bevel gear flank generation.

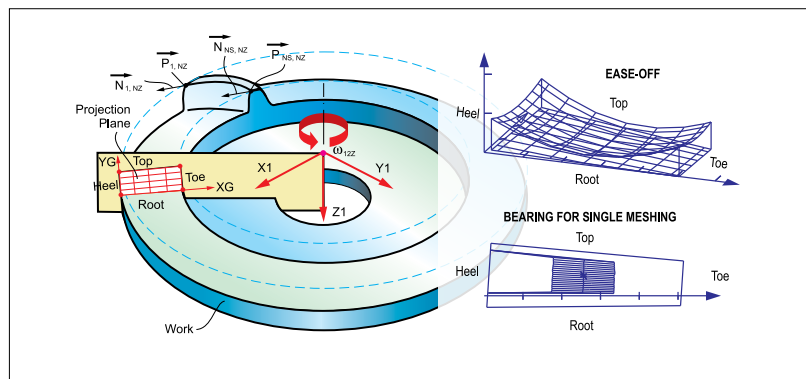


Figure 2—Definition of presentation plane.

Below the ease-offs, the motion transmission graphs of the particular mating flank pair are shown. If the pinion drives with a constant angular velocity, then the gear ideally should also rotate with a constant angular velocity but slower than the pinion by the factor of the gear ratio. The motion transmission graphs show the angular variation of the gear rotation from the ideal performance. In the present case of zero crowning, the motion transmission graph is a horizontal line (precise motion transmission).

The contact pattern at the bottom of Figure 3 shows contact lines (inside of the gear tooth projection) that extend throughout the active working area of the flank. This is also typical for conjugacy between pinion and gear flanks; however, such a conjugate tooth contact leads to edge contact as result of manufacturing tolerances and deflections under load.

Crowning has to be applied either to the pinion or gear—or both—in order to prevent edge contact along the boundaries of the teeth. Figure 4 shows TCA sequences of the three

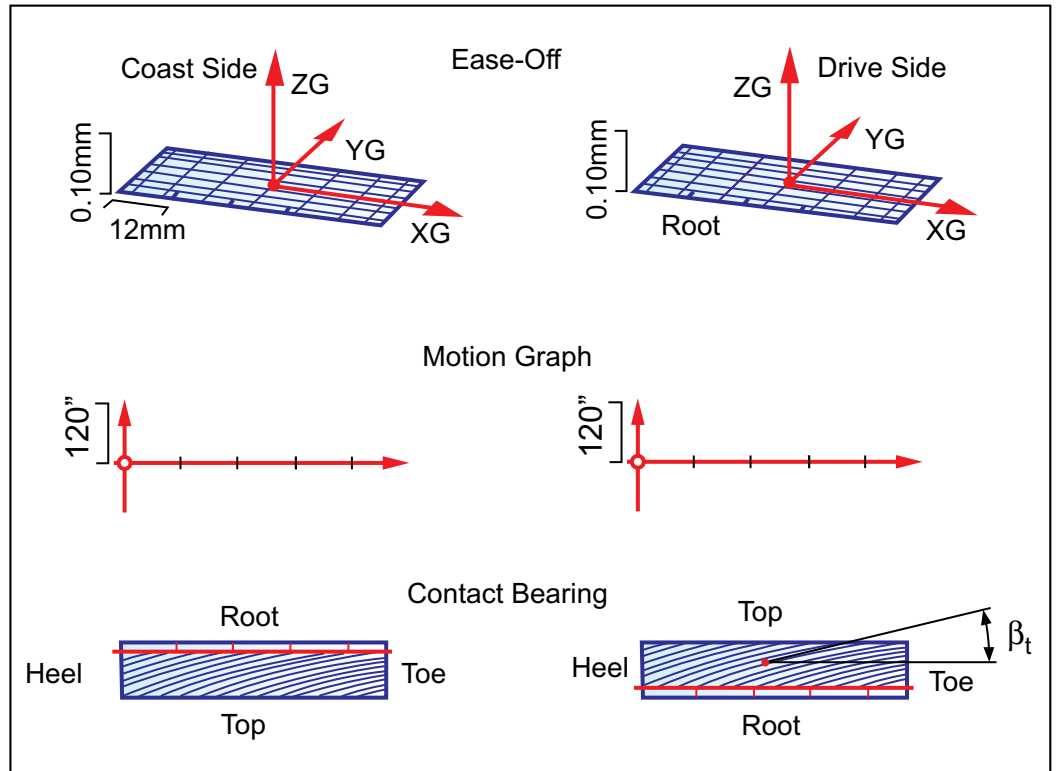


Figure 3—Tooth contact analysis of conjugate gear set.

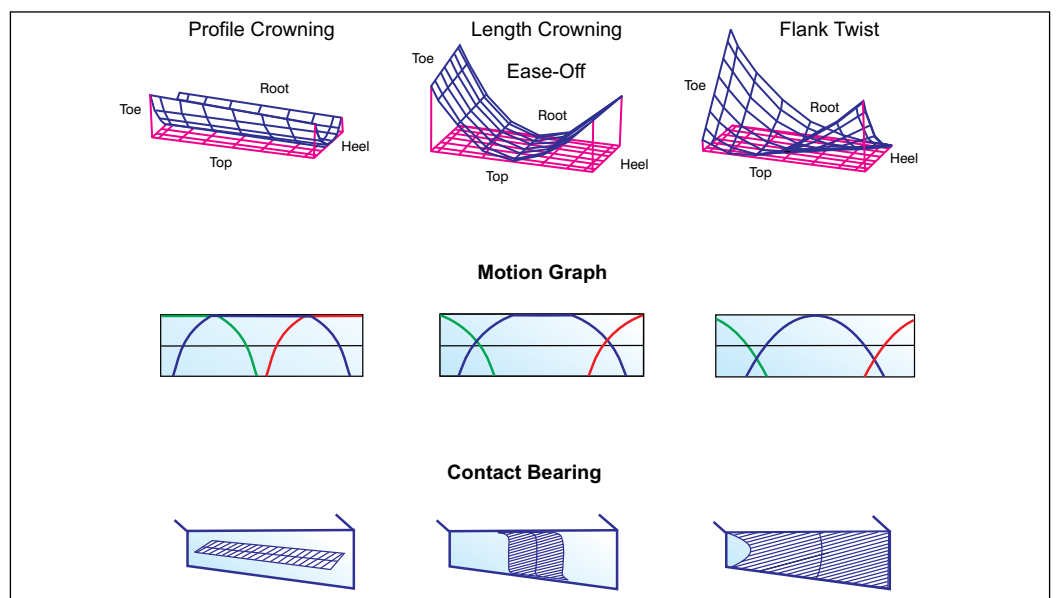


Figure 4—Tooth contact analysis with various types of crowning.

typical kinds of crowning. The top graphics show the ease-off topography. The surface above the presentation grid shows the consolidation of the pinion crowning portion and the gear crowning portion. The ease-offs in Figure 4 could be the result of pinion crowning only, or of the superimposition of a certain amount of both pinion and gear crowning.

Below each ease-off, the motion transmission graphs of the particular mating flank pair are shown. The graphs are drawn for the rotation and mesh of three consecutive pairs of teeth. While the ease-off requires reflecting a sufficient amount of crowning in order to prevent edge contact and allow for load-affected deflections, the crowning will in turn cause proportional amounts of maximal motion variation from zero.

At the bottom of Figure 4, the contact patterns are calculated for zero load and a virtual marking compound film of 6 μm thickness. This basically duplicates the tooth contact one would observe—i.e., rolling the real version of the analyzed gear set under light load on a roll tester while the gear member is coated with a marking compound layer of about 6 μm thickness. A smaller tooth contact area generally results from large magnitudes of ease-off and motion graph magnitudes, and vice versa. The parallel lines inside of the contact pattern are the contact lines for a number of discrete roll and contact positions between a pinion and a gear flank. The central line inside of the contact pattern is the path of contact, which is the sum of contact locations if the teeth are rolled with zero load. The left vertical sequence in Figure 4 is the analysis result of a pure profile crowning. The sequence in the center shows a pure length crowning and the right sequence is the result of a pure flank twist. Real bevel and hypoid gear sets consist generally of a mixture of these three crowning types.

Lubrication Gap Analysis

The basis of a lubrication gap analysis is the geometric and kinematic understanding of the interaction between the pinion and gear flank surfaces. Figure 5 (left side) shows a pinion flank rolling on a gear flank with a contact zone. The contact zone extends distance A along one pair of corresponding, potential contact lines between pinion and gear. While the gear set rotates in mesh, the contact zone will move from its current location—i.e., to the right. The relative surface curvatures between the two flanks are separated in two principal

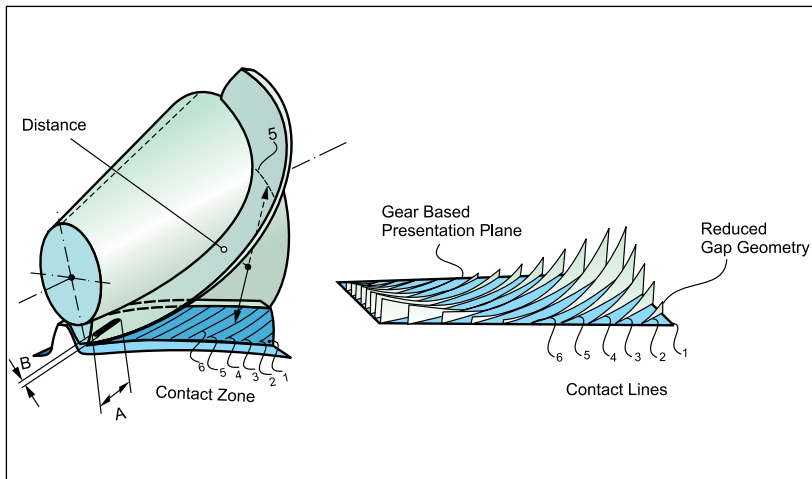


Figure 5—Two lubrication gap aspects.

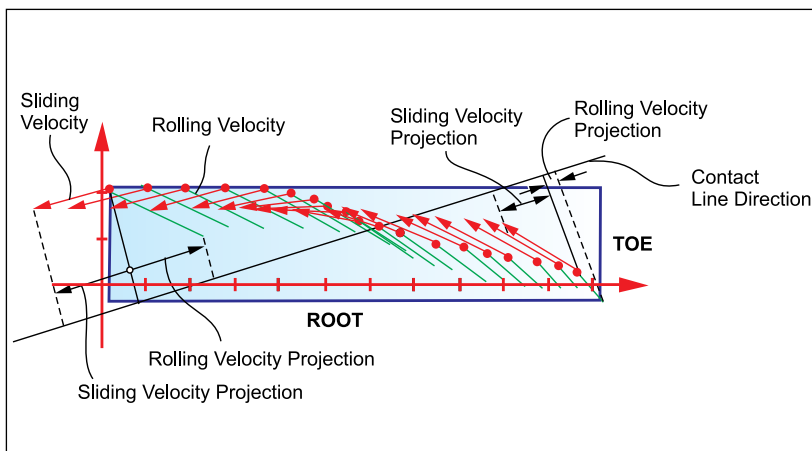


Figure 6—Sliding and rolling velocities of a hypoid gear set along the path of contact.

directions: one along the contact line and one along the path of contact, which is the direction from one contact line to the next. The curvature in the path-of-contact direction is some magnitudes larger than the curvature in contact-line direction, which is reflected by $A \gg B$. However, depending on the angle of the contact lines and on the direction of the sliding and rolling velocities between both flanks—both directions, contact line direction and the direction perpendicular to that (the latter is not always identical with the path-of-contact direction)—have to be considered for a hydrodynamic investigation. The right-side graphic in Figure 5 shows the reduced curvatures of 20 discrete contact lines, each in their contact position, plotted above the gear projection plane (contact line scan).

Figure 6 shows the sliding- and rolling-velocity vectors of a typical hypoid gear set for each path-of-contact point for the 20 discussed roll positions; each vector is projected to the tangential plane at the point of origin of the

continued

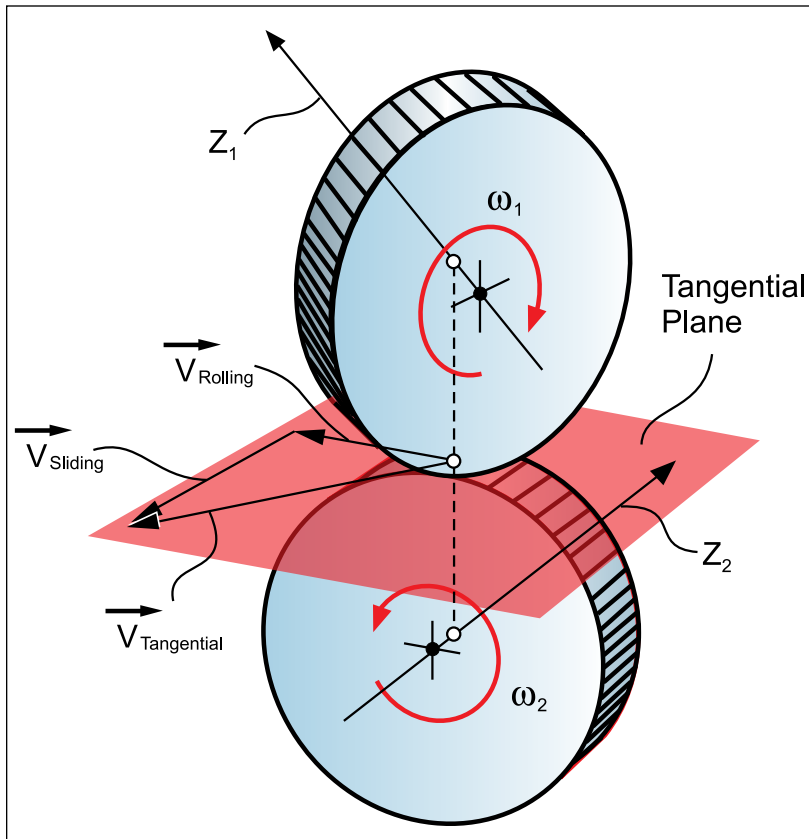


Figure 7—Definition of sliding and rolling velocity.

vector. The velocity vectors are drawn inside the gear tooth projection plane. The points of origin for both rolling- and sliding-velocity vectors are grouped along the path of contact, which is found as the connection of the minima of the individual lines in the contact line scan graphic (Fig. 5, right). An observer of one particular path-of-contact point on the gear flank surface would notice a momentarily contacting pinion point sliding away in the direction and with the speed represented by the sliding-velocity vector. The observer would also notice (particularly at the pitch point in straight bevel and spiral bevel gears, where no sliding and only rolling occurs) that the solid body connected to that point moved in a certain direction by rolling like a wheel rolls on pavement. The direction of this rolling and the movement accomplished via rolling (per time unit) are represented by the direction and magnitude of the rolling-velocity vector. Another way to explain the definition of rolling and sliding velocity in bevel and hypoid gears is shown in Figure 7. Disk 1 (top) rotates with ω_1 and is in contact with Disk 2 (bottom). The circumferential speed of Disk 1 is called the tangential velocity $V_{Tangential}$. The component of $V_{Tangential}$, which points in the axial direction of Disk 2, cannot rotate Disk 2—it only causes

a sliding $V_{Sliding}$. The component that points in tangential direction of Disk 2 $V_{Rolling}$ and causes Disk 2 to rotate with ω_2 is called the rolling velocity.

It is worth noting that the rolling velocities have a relatively consistent direction, while the sliding velocities change their direction along the path of contact significantly. Figure 6 shows the average directions of the contact lines. The sliding and rolling velocities are projected in the contact-line direction (see two example projections at left and right, Fig. 6). An analog projection in the direction perpendicular to the contact lines (not identical to the path-of-contact direction) allows two separate observations of the dynamics along the contact lines and perpendicular to them. The gap geometry change from contact line to contact line (Fig. 5, right) can be considered as an additional aspect. A single observation, for example, of the main direction seems to be unacceptable since sliding and rolling velocity have different directions and change along the path of contact significantly.

The answer to the question—Why is the split of sliding and rolling velocities proposed in the contact line direction and in a second component in the direction perpendicular to it, rather than in the path-of-contact direction—may not be obvious. The path of contact is not a principal curvature direction. Sliding and rolling velocities and the geometry of the contact line scan will move the contact from one path-of-contact point to the next. Small crowning changes will not influence the contact lines but will have great influence on the path-of-contact direction. The path of contact is an indirect gear set property that depends on the following parameters:

- sliding velocity (hypoid offset)
- rolling velocity (spiral angle)
- contact line orientation (spiral angle)
- characteristic of crowning (ease-off, contact-line crowning)

This phenomenon, which can only be observed in bevel and hypoid gears, derives from the fact that along the major contact movement (direction perpendicular to contact lines) the curvature of the lubrication gap is basically constant, but the velocities change. Whereas, in the contact-line direction, both curvature and velocities change constantly (Figs. 5–6).

Examples

The observation of this complex condition

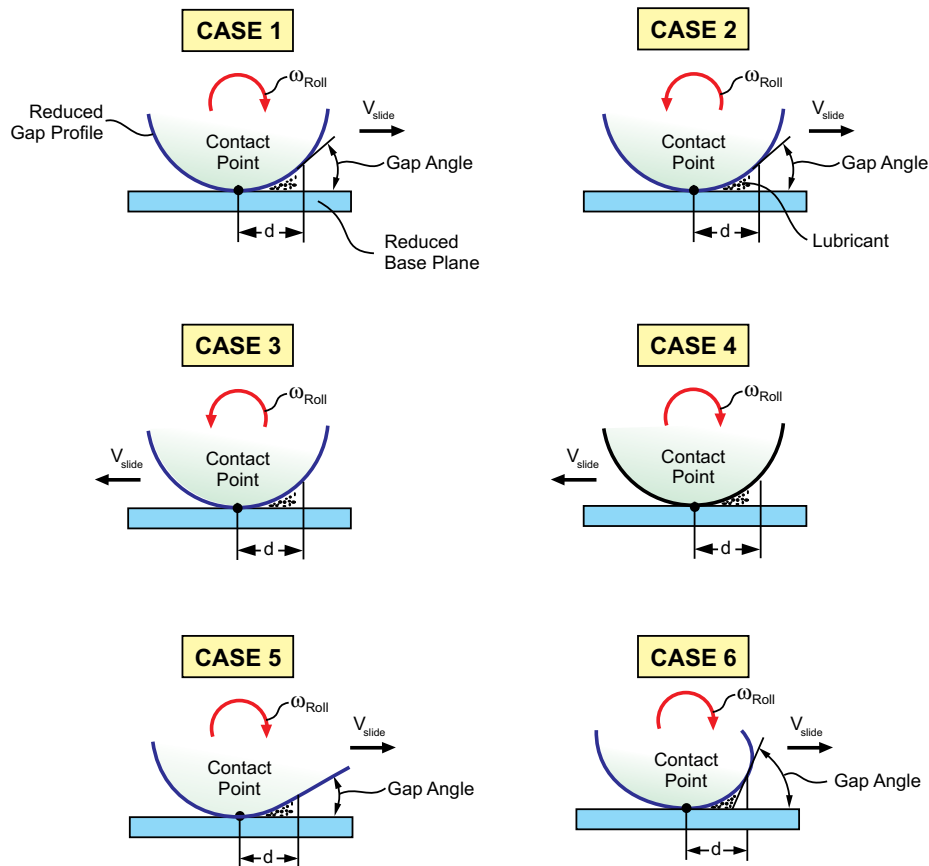


Figure 8—Six principal cases of lubrication gap kinematics.

leads to Figure 8, which shows six interesting cases of lubrication gap geometry and kinematics. Lubrication fluid is presented at right in each case drawing. Case 1 shows a clockwise rotation of a circular profile and a sliding to the right. This presents an enhancing condition for hydrodynamics. In Case 2 the rolling is reversed, thus reducing oil access to the lubrication gap. In Case 3 the sliding velocity and rotation are reversed, versus Case 1, thus presenting the most unfavorable kinematic lubrication condition. Case 4 has a reversed velocity direction versus Case 1 that presents a lubrication condition similar to Case 2. Cases 5 and 6 at bottom of Figure 8 are geometry variations that are applicable for the rolling and sliding directions indicated in Figure 6.

In Case 5 the curvature reduces while the profile rotates. This increases the lubricant pressure in front of the gap and will therefore enhance Case 1. In Case 6 a curvature increase is noticed while the rotation is progressing, which expands the lubrication gap. The latter will generate a vacuum that tends to pump the

lubricant away from the contact zone. Case 6 will reduce the lubrication quality. A simplified rating of the lubrication quality is proposed:

Very Good:

- a Case 5
- b Case 1
- c Case 6
- d Case 2
- e Case 4

Poor:

- f Case 3

A qualitative judgment of the lubrication case of a bevel or hypoid gear set is possible by comparing the contact line gaps (and their change during the rolling process) as well as the velocities with the principal cases shown in Figure 8.

With awareness of the rolling and sliding velocities within the flank surface area, every contact line and every path-of-contact point

continued

$$\{F_n\} = (F_x, F_y, F_z) \quad (1)$$

Tangential force F_x calculated from torque (2)

$$F_x = -T / (A_m \cdot \sin\gamma)$$

Rotation of vector normal to flank (3)

$$\{F_n\} = (90^\circ - \gamma)_X \cdot (\beta)_Z \cdot (\alpha)_Y \cdot (|F_n|, 0, 0)$$

Matrix multiplication of formula 3 and component solution

$$F_x = |F_n| \cdot \cos\beta \cdot \cos\alpha \quad (4)$$

$$F_y = |F_n| \cdot (\cos(90^\circ - \gamma) \cdot \sin\beta \cdot \cos\alpha + \sin(90^\circ - \gamma) \cdot \sin\alpha) \quad (5)$$

$$F_z = |F_n| \cdot (\sin(90^\circ - \gamma) \cdot \sin\beta \cdot \cos\alpha - \cos(90^\circ - \gamma) \cdot \sin\alpha) \quad (6)$$

Eliminate absolute value of F_n (7)

$$|F_n| = F_x / (\cos\beta \cdot \cos\alpha) = -T / (A_m \cdot \sin\gamma \cdot \cos\beta \cdot \cos\alpha)$$

Final solution of force components

$$F_x = -T / (A_m \cdot \sin\gamma) \quad (8)$$

$$F_y = -T \cdot (\sin\gamma \cdot \sin\beta \cdot \cos\alpha + \cos\gamma \cdot \sin\alpha) / (A_m \cdot \sin\gamma \cdot \cos\beta \cdot \cos\alpha) \quad (9)$$

$$F_z = -T \cdot (\cos\gamma \cdot \sin\beta \cdot \cos\alpha - \sin\gamma \cdot \sin\alpha) / (A_m \cdot \sin\gamma \cdot \cos\beta \cdot \cos\alpha) \quad (10)$$

where:

T	Torque of observed member
A_m	Mean cone distance
γ	Pitch angle
β	Spiral angle
α	Pressure angle
$\{F_n\}$	Normal force vector
$ F_n $	Absolute value of normal force
F_x, F_y, F_z	Bearing load force components

can be assigned to one case in Figure 8. It is also possible to use the reduced curvatures (which are contained in the contact line graphs) in connection with surface roughness and normal force distribution to establish a Stribeck graph and find contact conditions (boundary condition, mixed contact and hydrodynamic contact) in different cases and in different flank areas.

Proposed Bearing Forces Calculation

A formula derivation to calculate bearing forces is shown below. The formulas are based on the assumption that one pair of teeth transmits the torque with one normal force vector in the mean point of the flank pair. Figure 9 shows a graphical representation of the following derivation:

- The observed flank is rotated with the mean point into the horizontal Y-Z plane. The force F_x is the tangential force that transmits the torque. The normal force vector is found by a vector rotation from an X-orientation and in three steps—pressure angle, spiral angle and pitch angle—shown in Equation 3. With knowledge of the tangential component, the solution of Equation 7 can be plugged into Equations 4, 5 and 6 in order to find a universal solution in Equations 8, 9 and 10 for the bearing loads of one particular member. In the case of a right-hand, spiral-angle β , the sign is positive. In the case of a left-hand, spiral-angle β , the sign is negative. If the torque develops a force F_x pointing in contrast to Figure 9 to the positive X-direction, then α and T must be applied with a negative sign.

The results of the simplified bearing force calculation are good approximations and reflect the real bearing loads for multiple-tooth meshing within an acceptable tolerance. A precise calculation is, for example, possible with Gleason bevel and hypoid gear software. ⚙️

(Next issue—Hypoid Gears)

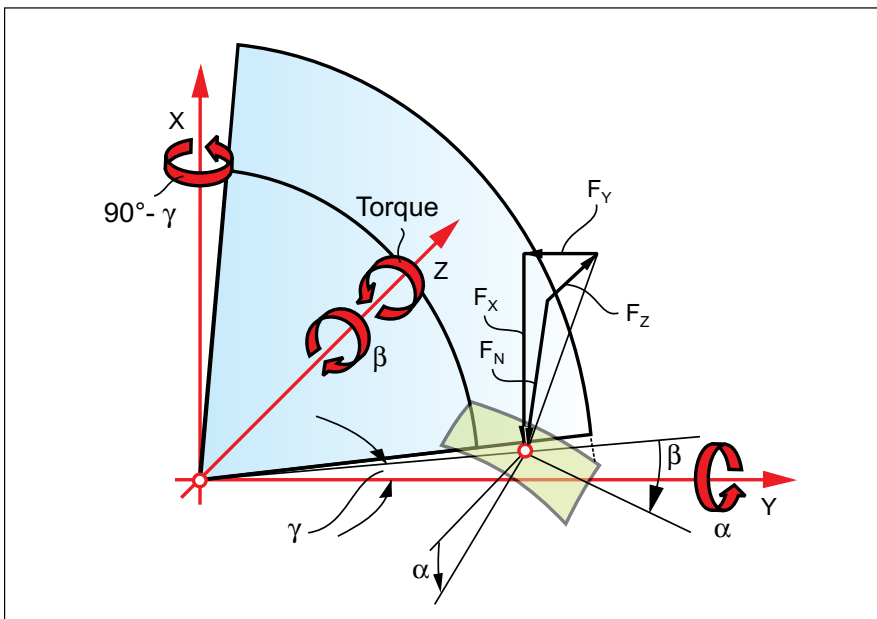


Figure 9—Bearing reaction load calculation.